Available online at www.sciencedirect.com
ScienceDirect
C. R. Mecanique 337 (2009) 268–276
COMPTES RENDUS MECANIQUE

Numerical study of deformation-induced fluid flows in periodic osteonal matrix under harmonic axial loading

Vu-Hieu Nguyen, Thibault Lemaire, Salah Naili *

Laboratoire de mécanique physique, université Paris 12, 61, avenue du Général de Gaulle, 94010 Créteil cedex, France

Received 3 April 2009; accepted after revision 22 June 2009

Available online 22 July 2009

Presented by Jean-Baptiste Leblond

Abstract

Living bone is a tissue that is constantly renewed. It has been demonstrated that bone fluid flow and induced shear effects on the bone cells are important players in triggering and signaling bone formation and remodelling. This Note presents a model studying interstitial fluid flow in cortical bone under axial harmonic loads. These living tissues are considered as saturated anisotropic poroelastic material characterized by three-dimensional periodic groups of osteons. Using a frequency-domain analysis, the fluid shear stress variations are studied for various loading conditions and geometrical or physical bone matrix parameters. ***To cite this article: V.-H. Nguyen et al., C. R. Mecanique 337 (2009).***

© 2009 Académie des sciences. Published by Elsevier Masson SAS. All rights reserved.

Keywords: Biomechanics; Osteon; Haversian bone; Mechanotransduction; Poroelasticity; Periodic; Harmonic loading; Finite element

1. Introduction

As a living tissue, cortical bone maintains and adapts its structure to external physical *stimuli* [1]. For instance, mechanical loading influences the rate of bone tissue renewal [2]. Linking bone mechanical loading to local bone tissue remodelling is a subject of great interest as it could help to better understand this phenomenon. Such a task requires to know the structural [3] and mechanical [4] properties of bone tissues. A poroelastic model of a single osteon, the structural cylindrical unit of cortical bone, was proposed in [5,6] to study the pore pressure and interstitial fluid flow in cortical bone matrix. It illustrated the high dependency of the osteon hydraulic behaviour on poroelastic parameters as well as on the loading conditions. Nevertheless, in these studies, the surrounding cement layer of the osteon (cement line) was assumed to be perfectly rigid and impermeable. This assumption may be rough since micropores of osteonal tissues do cross cement lines [7]. As a consequence, mechanical behaviour of the osteon might be influenced by its surrounding environment.

The aim of this Note is to propose a model to study how a mechanical *stimulus* involved in bone remodelling process changes with various loading conditions and geometrical or physical bone matrix parameters. Section 2 begins

* Corresponding author.
E-mail address: naili@univ-paris12.fr (S. Naili).

1631-0721/$ – see front matter © 2009 Académie des sciences. Published by Elsevier Masson SAS. All rights reserved.
doi:10.1016/j.crme.2009.06.033

with a description of the model which considers the bone matrix as a periodic array of osteons. Then, the governing equations are introduced. They are based on Biot's poroelastic theory applied to three-dimensional anisotropic media. Moreover, assuming the homogeneous deformation in the longitudinal direction, a two-dimensional system can be deduced. Section 3 presents a method of resolution of the problem in the frequency domain and Section 4 provides some numerical results in terms of hydraulic behaviour of the fluid.

2. Statement of the problem

2.1. Three-dimensional geometrical description and governing poroelastic equations

In the osteonal bone matrix, Haversian canals run longitudinally through the bone cortex and are transversely inter-connected by Volkmann canals. Osteon consists of a matrix of layers called lamellae which are developed concentrically around one Haversian canal and presents a cylinder-like form. Osteocytes are found between concentric lamellae and connected to each other and the central canal by cytoplasmic processes through the canals called *canaliculi*. This network permits the exchange of nutrients and metabolic waste [4]. Each osteon is coated by a thin layer called the cement line. The tissues found outside of the cement lines, *i.e.* tissues that fill the space between the osteons, are old osteonal matrix called interstitial osteons.

The cement line of secondary osteon presents a front where the bone removal activity associated with construction of a new osteon has ceased and bone deposition activity begins. The nature of the cement line is not really known and is still in debated. For instance, Burr et al. [8] suggested that the cement lines of secondary osteons are poorly mineralized while Skedros et al. [9] found that cement line represents relatively hypermineralization.

For simplification purposes, the osteonal zone considered here is assumed to be located far enough from transverse Volkmann canals, so that their influence can be neglected. Fig. 1-A shows a representative matrix of osteons containing Haversian canals that run in the vertical direction $\boldsymbol{x}_3$. Thus, osteons are depicted as thick-walled hollow cylinders. They are assumed to be identical and parallel. Moreover, they are arranged periodically in the horizontal plane $(\boldsymbol{x}_1, \boldsymbol{x}_2)$ (see Fig. 1-B).

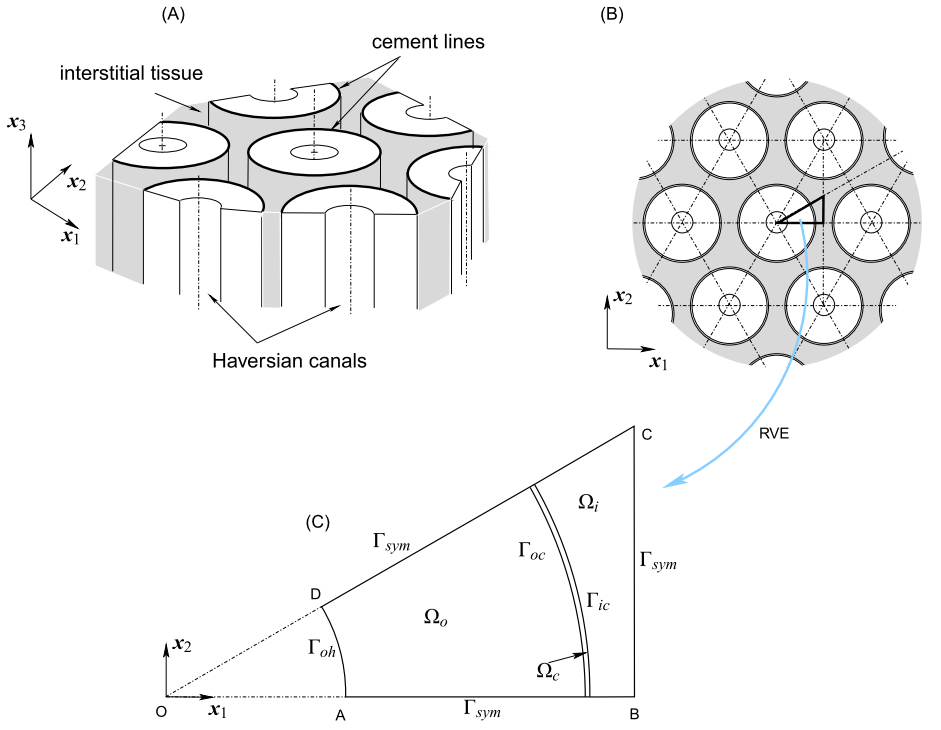

Fig. 1. An idealized periodic array of osteons.

All those bone materials (osteons, cement lines, interstitial tissues) are considered as linear saturated anisotropic poroelastic media. The influence of canaliculae (as well as of lacunae) is taken into account through the homogenized permeability and the porosity of the porous domain. No body forces are considered. For low frequencies, the equations of the anisotropic poroelastic medium are given by [10,11]:

$$\rho \ddot{\boldsymbol{u}} - \operatorname{div} \boldsymbol{\sigma} = \mathbf{0} \tag{1}$$

$$\frac{1}{M}\dot{p} - \operatorname{div}(\boldsymbol{k} \operatorname{grad} p) + \boldsymbol{\alpha} : \dot{\boldsymbol{\epsilon}} = 0 \tag{2}$$

where $\rho = \phi\rho_f + (1-\phi)\rho_s$ is the mixture density defined from the porosity ϕ and the densities of fluid and solid phases (ρ_f and ρ_s respectively), $\boldsymbol{u}$ and $\boldsymbol{\epsilon}$ are respectively the displacement vector and the strain tensor of the solid skeleton, $\boldsymbol{\sigma}$ is the total stress tensor, p is the fluid pressure in full-filled pores, $\boldsymbol{k}$ is the anisotropic permeability tensor, $\boldsymbol{\alpha}$ is the Biot tensor and M is the Biot *modulus*. The derivatives with respect to the time t are denoted by superposed dot, the divergence and gradient operators are respectively denoted by div and grad. The symbol ':' between two quantities defines the scalar product in the appropriate space.

In what follows, the intrinsic permeability $\boldsymbol{\kappa}$ is used which is defined by $\boldsymbol{k} = \boldsymbol{\kappa}/\eta$, where η is the pore fluid dynamic viscosity. Moreover, the vector and tensor components are respectively denoted by u_i for $i = 1, \ldots, 3$ and σ_{ij} for $i, j = 1, \ldots, 3$ for instance for the displacement vector and the stress tensor.

Moreover, the stress and strain tensors and the pressure are linked by the relation:

$$\boldsymbol{\sigma} = \mathbb{C} : \boldsymbol{\epsilon} - \boldsymbol{\alpha} p \tag{3}$$

where $\mathbb{C}$ is the elastic stiffness tensor of drained material. For an orthotropic material, $\mathbb{C}$ is defined by 9 independent parameters; the tensors $\boldsymbol{\alpha}$ and $\boldsymbol{k}$ are assumed diagonal in the three principal directions and can be defined by 3 independent values.

2.2. Two-dimensional formulation

In the scope of this study, the considered tissues are assumed to be located in the diaphysial region a femur or tibia. Under walking activity, this region is essentially loaded following the long axis of bone which is also the direction of the Haversian canals. As a consequence, we are interested essentially in studying mechanical behaviour of the system in response to uniform axial loading in the $\boldsymbol{x}_3$-direction. Thus, some additional assumptions are made:

(H1) The excitation applied on the system in the vertical direction is uniform and thus the vertical displacement in an arbitrary horizontal plane is assumed to be uniform: $\frac{\partial u_3}{\partial x_1} = \frac{\partial u_3}{\partial x_2} = 0$;
(H2) The low-frequency excitation applied on the structure is considered as a cyclic loading (*i.e.* the dimension of the structure is very small in comparison with the wave length): $\frac{\partial u_1}{\partial x_3} = \frac{\partial u_2}{\partial x_3} = 0$;
(H3) The size of the longitudinal cross section of the domain is sufficiently large in comparison with the size of one osteon cross section and thus we can neglect boundary effects when considering osteons in the middle of the domain.

The assumptions (H1) and (H2) imply that there are no shear strains in two vertical planes $(\boldsymbol{x}_1, \boldsymbol{x}_3)$ and $(\boldsymbol{x}_2, \boldsymbol{x}_3)$, *i.e.* $\epsilon_{13} = \epsilon_{23} = 0$. As a consequence $\sigma_{13} = \sigma_{23} = 0$. Applying these conditions to the system of Eqs. (1) and (2) and neglecting the term related to $\ddot{\epsilon}_{33}$, a two-dimensional problem is obtained:

$$\rho \ddot{u}_1 - \frac{\partial \sigma_{11}}{\partial x_1} - \frac{\partial \sigma_{12}}{\partial x_2} = 0 \tag{4}$$

$$\rho \ddot{u}_2 - \frac{\partial \sigma_{12}}{\partial x_1} - \frac{\partial \sigma_{22}}{\partial x_2} = 0 \tag{5}$$

$$\frac{1}{M}\dot{p} - k_{11}\frac{\partial^2 p}{\partial x_1^2} - k_{22}\frac{\partial^2 p}{\partial x_2^2} - 2k_{12}\frac{\partial^2 p}{\partial x_1 \partial x_2} + \alpha_{11}\dot{\epsilon}_{11} + \alpha_{22}\dot{\epsilon}_{22} + 2\alpha_{12}\dot{\epsilon}_{12} + \alpha_{33}\dot{\epsilon}_{33} = 0 \tag{6}$$

where

$$\sigma_{11} = c_{11}\frac{\partial u_1}{\partial x_1} + c_{12}\frac{\partial u_2}{\partial x_2} + c_{13}\epsilon_{33} - \alpha_{11}p, \quad \sigma_{22} = c_{21}\frac{\partial u_1}{\partial x_1} + c_{22}\frac{\partial u_2}{\partial x_2} + c_{23}\epsilon_{33} - \alpha_{22}p \tag{7}$$

$$\sigma_{12} = c_{44}\left(\frac{\partial u_1}{\partial x_2} + \frac{\partial u_2}{\partial x_1}\right) \tag{8}$$

The 4-by-4 matrix $\mathbf{c}$ is built from the elasticity tensor $\mathbb{C}$; these components c_{ij} (for $i, j = 1, \ldots, 4$) are given by:

$$\mathbf{c} = \begin{bmatrix} C_{1111} & C_{1122} & C_{1133} & 0 \\ C_{2211} & C_{2222} & C_{2233} & 0 \\ C_{3311} & C_{3322} & C_{3333} & 0 \\ 0 & 0 & 0 & C_{1212} \end{bmatrix} \tag{9}$$

By taking advantage of periodicity of the array of osteons, the Representative Elemental Volume (REV) is defined by the domain ABCD in which AD is Haversian canal's wall and AB, BC, CD are the *symmetrical boundaries* wherein symmetric conditions are considered (see Fig. 1-C).

2.3. Interface and boundary conditions

The interface and symmetry conditions are now presented. Some superscripts referring to different material components of the cortical medium are introduced in association with the different fields: Haversian canal (h), osteon (o), cement line (c) and interstitial tissues (i). Moreover, the coordinates of the normal unit vector of the interface $\Gamma_{\alpha\beta}$ between the domains (α) and (β) are noted $n_j^{\Gamma_{\alpha\beta}}$.

(i) As we are interested in the behaviour of the osteon under bone deformation due to activities like running or walking, the induced variation of fluid pressure in lacunar–canalicular pores is much higher than the one in the vascular pores. Here, the reference pressure is considered and the surface is then assumed to be free at the interface between osteon and Haversian canal ($\boldsymbol{x} \in \Gamma_{oh}$):

$$p^{(o)} = 0 \quad \text{and} \quad \sigma_{ij}^{(o)} n_j^{\Gamma_{oh}} = 0 \tag{10}$$

(ii) At the interface between the osteon and the cement line ($\boldsymbol{x} \in \Gamma_{oc}$), the pressure, displacement, normal velocity, and normal stress are continuous:

$$p^{(o)} = p^{(c)} \quad \text{and} \quad u_i^{(o)} = u_i^{(c)} \tag{11}$$

$$-k_{ij}^{(o)}\frac{\partial p^{(o)}}{\partial x_j} n_i^{\Gamma_{oc}} = -k_{ij}^{(c)}\frac{\partial p^{(c)}}{\partial x_j} n_i^{\Gamma_{oc}} \quad \text{and} \quad \sigma_{ij}^{(o)} n_j^{\Gamma_{oc}} = \sigma_{ij}^{(c)} n_j^{\Gamma_{oc}} \tag{12}$$

(iii) At the interface between the cement line and the interstitial tissue ($\boldsymbol{x} \in \Gamma_{ci}$), the pressure, displacement, normal velocity and normal stress are continuous (analogous equations as relations (11) and (12)).

(iv) At the symmetric boundary $\boldsymbol{x} \in \Gamma_{sym}$, the normal pressure flux and displacement are zero:

$$\frac{\partial p}{\partial x_i} n_i^{\Gamma_{sym}} = 0 \quad \text{and} \quad u_i n_i^{\Gamma_{sym}} = 0 \tag{13}$$

3. Equations in the frequency domain

The vertical strain is assumed to be a time-harmonic function which can be expressed by $\epsilon_{33} = \epsilon_0 e^{i\omega t}$, where ϵ_0 is the strain amplitude and ω is the angular frequency of loading. Since we only focus on the stationary response of the system, a transformation into the frequency domain is carried out. Thus, the solutions of $\boldsymbol{u}$ and p are investigated using the forms $\boldsymbol{u}(x_1, x_2, t) = \hat{\boldsymbol{u}}(x_1, x_2)e^{i\omega t}$ and $p(x_1, x_2, t) = \hat{p}(x_1, x_2)e^{i\omega t}$. Transposing these expressions in the system (4)–(6) and simplifying the term $e^{i\omega t}$, a two-dimensional system of differential equations is obtained:

$$-\omega^2\rho\hat{u}_1 - \frac{\partial\hat{\sigma}_{11}}{\partial x_1} - \frac{\partial\hat{\sigma}_{12}}{\partial x_2} = 0 \tag{14}$$

$$-\omega^2\rho\hat{u}_2 - \frac{\partial\hat{\sigma}_{12}}{\partial x_1} - \frac{\partial\hat{\sigma}_{22}}{\partial x_2} = 0 \tag{15}$$

$$\frac{i\omega}{M}\hat{p} - k_{11}\frac{\partial^2\hat{p}}{\partial x_1^2} - k_{22}\frac{\partial^2\hat{p}}{\partial x_2^2} - 2k_{12}\frac{\partial^2\hat{p}}{\partial x_1\partial x_2} + i\omega(\alpha_{11}\hat{\epsilon}_{11} + \alpha_{22}\hat{\epsilon}_{22} + 2\alpha_{12}\hat{\epsilon}_{12}) = -i\omega\alpha_{33}\epsilon_0 \tag{16}$$

where

$$\hat{\sigma}_{11} = \tilde{c}_{11}\frac{\partial\hat{u}_1}{\partial x_1} + \tilde{c}_{12}\frac{\partial\hat{u}_2}{\partial x_2} + \tilde{c}_{13}\epsilon_0 - \alpha_{11}\hat{p}, \quad \hat{\sigma}_{22} = \tilde{c}_{21}\frac{\partial\hat{u}_1}{\partial x_1} + \tilde{c}_{22}\frac{\partial\hat{u}_2}{\partial x_2} + \tilde{c}_{23}\epsilon_0 - \alpha_{22}\hat{p} \tag{17}$$

$$\hat{\sigma}_{12} = \tilde{c}_{44}\left(\frac{\partial\hat{u}_1}{\partial x_2} + \frac{\partial\hat{u}_2}{\partial x_1}\right) \tag{18}$$

4. Numerical results

The weak formulations of previous equations have been derived and implemented into the finite element software COMSOL MULTIPHYSICS [12].

By using these formulations, some relevant tests have been carried out to investigate the hydraulic sensibility of the system in function of (i) the amplitude and the frequency of the loading; (ii) the permeability of the cement lines; (iii) the distance between osteons. According to [13], the mechanosensitive cells of cortical bone, the osteocytes, are sensitive to induced fluid shear stress acting on their membranes. This *stimulus* would be a key element in bone remodelling process [1]. As a consequence, the hydraulic behaviour of the bone tissue is essentially described in terms of shear stress. These microscopical shear effects are proportional to macroscopic fluid velocities and may be estimated using the procedure proposed in [14].

As we have discussed below, in this study, the presence of lacunar–canalicular pores are introduced through the porosity and permeability parameters. Moreover, this study focuses on the mechanosensitive osteocyte cells embedded in the osteonal matrix in the lacunae. Typically, these cells present a body of a few micrometers and communicate one with another thanks to cytoplasmic processes (around 0.1 μm of radius) developing in the canalicular network. Due to mass conservation arguments, the cell–fluid interactions are supposed to be relevant at the canalicular scale (see [15]). As a result, all the localisation results are presented at this scale.

4.1. Numerical parameters and numerical tests

The mechanical properties of the osteonal tissue strongly depend on its hierarchical organisation (see [16]). In this study, a reference structural configuration is assumed and the parameter values associated with this configuration are based on the literature [4]. The geometry is defined by: the inner (Haversian canal) and the outer radii of osteons, $r_i = 50$ μm and $r_o = 150$ μm respectively, the cement line thickness of 1 μm and the centre to centre distance between two osteons $2r_o + d$. As a result, the REV corresponding to the domain ABCD (see Fig. 1-C) is characterized by $OA = r_i$, $OB = r_o + d/2$ and $\measuredangle(OA, OD) = \pi/6$. In what follows, the material properties of the different subdomains of the REV are taken identical and are provided in Table 1. Nevertheless, the textural properties of the cement line are not the same as the ones of its neighbouring osteonal tissues. Thus, assuming isotropic permeability tensors, osteonal permeability parameters $\kappa^{(o)}$ and $\kappa^{(i)}$ are constant as stated in Table 1 whereas different values of the intrinsic permeability of the cement line $\kappa^{(c)}$ are studied.

Moreover, the load corresponds to an imposed vertical strain $\epsilon_{33} = \epsilon_0 e^{i\omega t}$ where ϵ_0 is the peak-to-peak magnitude. Noting f_0 the loading frequency, the role of the strain rate $\dot{\epsilon} = \epsilon_0 f_0$ is also discussed hereafter.

Table 1
Physical parameters considered for the tests (see [4]).

ρ_s (kg m^{-3})	E_1 (GPa)	E_2 (GPa)	E_3 (GPa)	G_{12} (GPa)	G_{13} (GPa)	G_{23} (GPa)	ν_{12} –	ν_{13} –	ν_{23} –
2000	15.9	E_1	20.3	$\frac{C_{11}-C_{12}}{2}$	6.9	6.9	0.328	0.25	ν_{13}
ρ_f (kg m^{-3})	ϕ –	α_1 –	α_2 –	α_3 –	κ_1 (m^2)	κ_2 (m^2)	κ_3 (m^2)	η (Pa s)	M (GPa)
1000	0.05	0.132	α_1	0.092	10^{-18}	10^{-18}	10^{-18}	10^{-3}	38.0

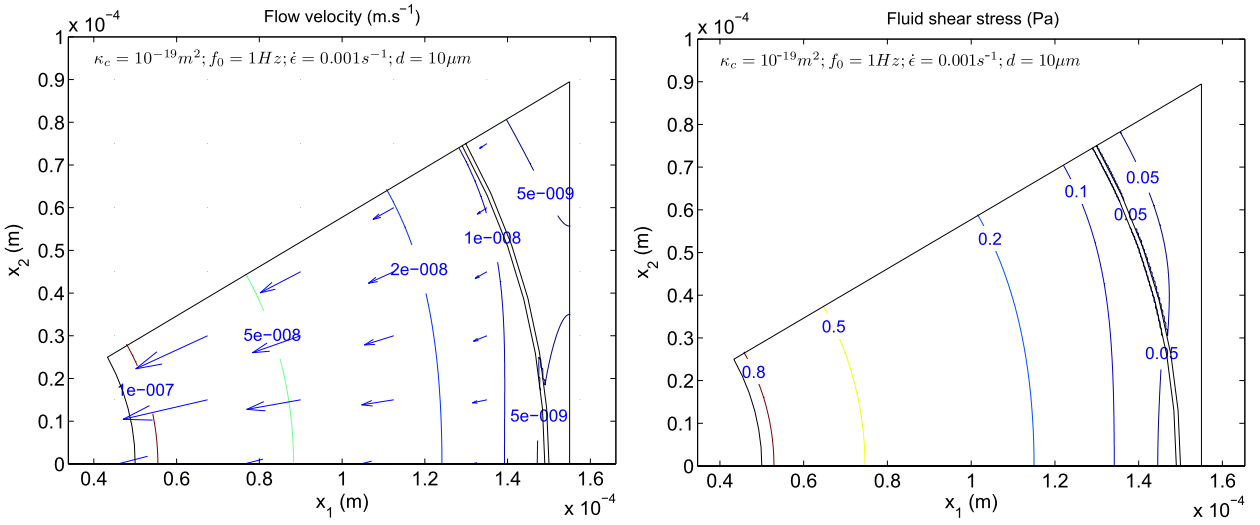

Fig. 2. Simulation of the fluid flow velocities (left) and shear fluid stress (right).

4.2. *Results and discussion*

4.2.1. *Behaviour of the fluid in bone matrix*

Fig. 2 presents a first case that illustrates the hydraulic behaviour of the system and can be used as a comparison point for the following results. Here, the cement line is less permeable in comparison with the osteon and interstitial tissues ($\kappa^{(c)} = 10^{-19}$ m^2). The frequency of loading $f_0 = 1$ Hz (that corresponds to walking activity) and strain rate $\dot{\epsilon} = 10^{-3}$ s^{-1} are taken to be typical of daily activity values. The inter osteons distance is $d = 10$ μm. The finite element mesh used in the simulation consists of 1797 triangular elements and 24 618 degrees of freedom.

On the left, the isovalue curves of maximal fluid velocity field in the compressional phase of the loading are plotted. In the compressional phase, pores volumes tend to be reduced making pore fluid pressure increases, then the fluid is pumped to flow toward the Haversian canal. The fluid velocity is more important at the Haversian edge and tends to nearly vanish at the vertical symmetric boundary. According to the Darcy law, the pressure inversely increases from its Haversian reference to reach its maximum in the interstitial tissues. Moreover, the velocity field as well as the pressure in the osteon are nearly axisymmetric close to the Haversian canal.

According to [17], bone cells *in vitro* actually respond to fluid shear stresses of 0.2–6 Pa over their surface. Thus our results would imply that under this specific loading condition, the osteon cells are only stimulated in the vicinity of the Haversian system (see Fig. 2, right). Indeed the osteocytes located near the cement line or in the interstitial tissues are not stimulated enough. We might suggest that there is a quite extensive hydraulic "dead zone" within the cortical tissue for the considered parameters.

4.2.2. *Effects of loading frequency and strain rate*

Fig. 3 presents two isovalue curves of the fluid-induced shear stress that aim at studying the influence of the loading frequency and strain rate. The same geometrical and physical parameters as in the precedent case are used.

We present in Fig. 3 (left) the case in which the loading frequency ($f_0 = 1$ Hz) is increased whereas the strain rate value is preserved ($\dot{\epsilon} = 0.001$ s^{-1}). A comparison with Fig. 2 shows that the differences of shear stress between lower- and higher-frequency cases are moderate.

The graph presented on Fig. 3 (right) shows that the fluid shear stress field is considerably modified when increasing the strain rate ($\dot{\epsilon} = 0.003$ s^{-1}) and fixing the loading frequency. This high dependency with the strain rate recovers the theoretical statements of [6,18] and the experimental observations presented by [19]. As a consequence, the previous hydraulic "dead zone" is limited to the interstitial tissues.

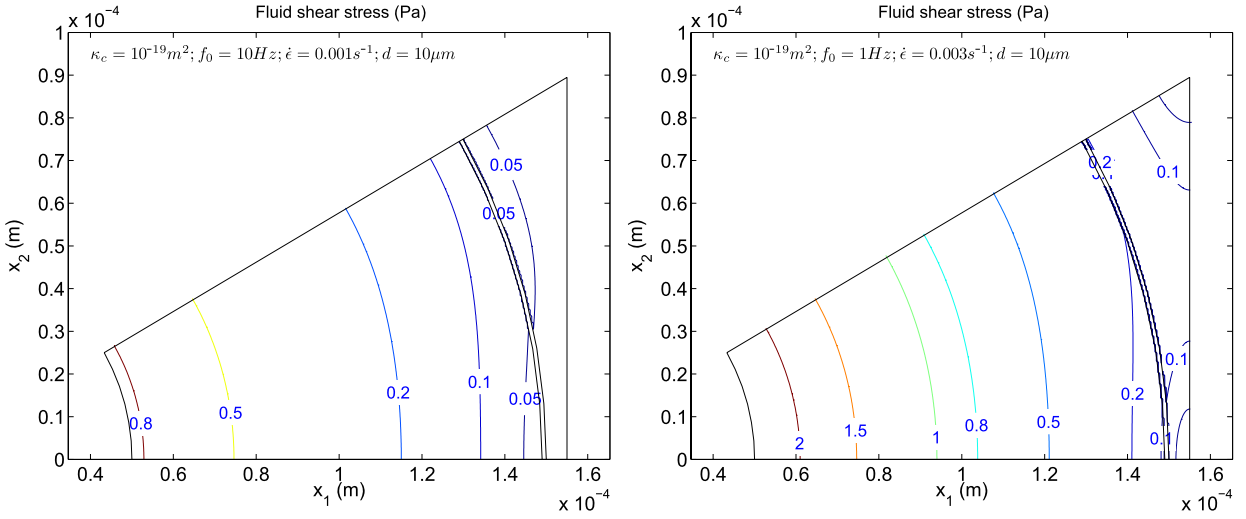

Fig. 3. Effects of frequency and strain rate.

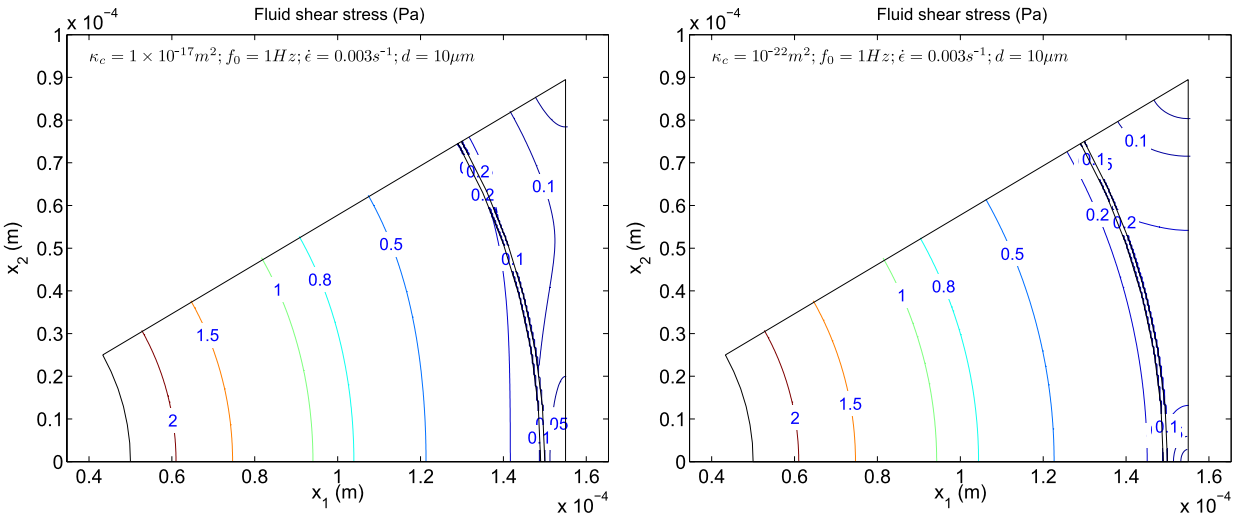

Fig. 4. Effects of the permeability of the cement lines.

4.2.3. Effects of the permeability of the cement lines

All those previous tests were performed assuming a cement line that is less permeable than the osteon and interstitial tissues. Keeping the most favorable loading condition ($f_0 = 1$ Hz and $\dot{\epsilon} = 0.003$ s^{-1}), two other cases are carried out on Fig. 4 to capture the cement line permeability influence: (i) the cement line is more permeable ($\kappa^{(c)} = 10^{-17}$ m^2); (ii) the cement line is impermeable ($\kappa^{(c)} = 10^{-22}$ m^2). This second value is a purely numerical criterion aiming at representing an impervious property since such a low permeability is physically unrealistic. A comparison between the second graph of Fig. 3 and the two graphs of Fig. 4 only shows slight differences for the shear stress in the vicinity of the cement line. Hence, the permeability of the cement line does not seem to play an important role in the shear stress distribution. Moreover, for the second case, the isovalue curves are axisymmetric because of the impermeability of the cement line.

4.2.4. Effects of the geometry

To finish our investigations, the interaction between osteons has been studied increasing the distance between two osteons: $d = 50$ μm (see Fig. 5). Compared to the second graph of Fig. 3 where $d = 10$ μm, the fluid shear effects are more important and a small area of the interstitial tissues is also stimulated.

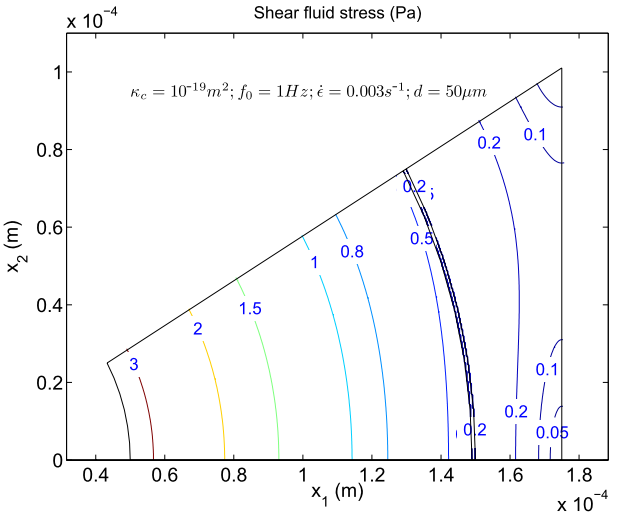

Fig. 5. Effects of the distance between osteons.

5. Conclusion and perspectives

Based on the poroelasticity theory, the investigation of hydraulic behaviour of cortical bone proposed in this study puts into relief some key-elements in the viewpoint of bone remodelling mechanotransduction: (i) as classically stated, the hydraulic remodelling signals depend strongly on strain rate; (ii) the permeability of the cement line does not strongly influence these signals; (iii) these signals are more sensitive to the osteons interactions, that is to say to the proximity between Haversian canals. This last point suggests that the distribution of vasculature in the bone volume is an important parameter in interstitial bone fluid movements. Thus, this work has to be pursued by taking into account the Volkmann canals and possible macrocracks. This will require us to adopt a 3-D treatment of the problem.

References

[1] T. Lemaire, S. Naïli, Stimuli physiques du remodelage osseux, in: Reconstruction osseuse et cutanée : Biomécanique et Techniques de l'Ingénieur, Sauramps Medical, 2008, pp. 57–71.
[2] L.E. Lanyon, C.T. Rubin, Static vs dynamic loads as an influence on bone remodelling, J. Biomech. 17 (12) (1984) 897–905.
[3] M. Predoi-Racila, C. Stroe, J.-M. Crolet, SiNuPrOs : Etude de la perméabilité multi-échelle de l'os cortical humain, in: Reconstruction osseuse et cutanée : Biomécanique et Techniques de L'ingénieur, Sauramps Medical, 2008, pp. 13–23.
[4] S.C. Cowin, Bone Mechanics Handbook, 2nd edition, CRC Press, Boca Raton, FL, 2001.
[5] A. Rémond, S. Naili, Transverse isotropic poroelastic osteon model under cyclic loading, Mech. Res. Comm. 32 (2005) 645–651.
[6] A. Rémond, S. Naili, T. Lemaire, Interstitial fluid flow in the osteon with spatial gradients of mechanical properties: A finite element study, Biomech. Model. Mechanobiol. 7 (2008) 487–495.
[7] T.A. Curtis, S.H. Ashrafti, D.F. Weber, Canalicular communication in the cortices of human long bone, Anat. Rec. 212 (1985) 336–344.
[8] D.B. Burr, M.B. Schaffler, R.G. Frederickson, Composition of the cement line and its possible mechanical role as a local interface in human compact bone, J. Biomech. 21 (11) (1988) 939–945.
[9] J.G. Skedros, L.H. Jennifer, E.G. Vajda, D.B. Roy, Cement lines of secondary osteons in human bone are not mineral-deficient: New data in a historical perspective, Anatomical Record Part A: Discoveries in Molecular, Cellular and Evolutionary Biology A 286 (1) (2005) 781–803.
[10] M.A. Biot, Theory of propagation of elastic waves in a fluid-saturated porous solid. I. Low-frequency range, J. Acoust. Soc. Am. 28 (1956) 168–178.
[11] A.H. Cheng, Material coefficients of anisotropic poroelasticity, Int. J. Rock Mech. Mining Sci. 34 (2) (1997) 199–205.
[12] COMSOL Multiphysics, Model library, Grenoble (France), 2005.
[13] I. Westbroek, N.E. Ajubi, M.J. Ablas, C.M. Semeins, J. Klein-Nulend, E.H. Burger, P.J. Nijweide, Differential stimulation of prostaglandin g/h synthase-2 in osteocytes and other osteogenic cells by pulsating fluid flow, Biochem. Biophys. Res. Commun. 268 (2000) 414–419.
[14] T. Lemaire, F. Borocin, S. Naili, Mechanotransduction of bone remodelling: role of micro-cracks at the periphery of osteons, C. R. Mecanique 336 (2008) 354–362.
[15] Y. Han, S.C. Cowin, M.B. Schaffler, W. Sheldon, Mechanotransduction and strain amplification in osteocyte cell processes, Proc. Natl. Acad. Sci. 101 (47) (2004) 16689–16694.

[16] M. Racila, J.M. Crolet, Nano and macro structure of cortical bone: Numerical investigations, Mech. Adv. Mater. Struct. 14 (8) (2007) 655–663.
[17] S.C. Cowin, Mechanosensation and fluid transport in living bone, J. Musculoskel Neuron Interaction 2 (3) (2002) 256–260.
[18] V.-H. Nguyen, T. Lemaire, S. Naili, Anisotropic poroelastic hollow cylinders with damaged periphery under harmonically axial loading: Relevance to bone remodelling, Multidiscipline Modeling in Materials and Structures 5 (2009) 205–222.
[19] C.H. Turner, Three rules for bone adaptation to mechanical stimuli, Bone 23 (5) (1998) 399–407.